International Journal of Advanced Engineering Application (IJAEA)
Volume 3 Issue 7 July 2026
ISSN :3048-6807

Mechanical, Fatigue, and Dimensional Performance of 3D-Printed PETG-Carbon Fiber Lattice Structures for Lightweight Automotive Mounting Brackets

Aditya N. Rao
Department of Mechanical and Industrial Engineering, National Institute of Technology, Pune, India

Abstract

The automotive industry's pursuit of mass reduction without compromising structural reliability has renewed interest in fused filament fabrication (FFF) of fiber-reinforced thermoplastics with internally engineered lattice architectures, since topology-optimised infill can deliver favourable stiffness-to-weight ratios unattainable in solid machined or injection-moulded parts while remaining compatible with low-volume production runs typical of aftermarket and motorsport bracket manufacturing. This study characterises the compressive, fatigue, thermal, and dimensional behaviour of carbon-fiber-reinforced PETG (PETG-CF, 15 wt% short fiber) printed with three unit-cell lattice topologies — gyroid (triply periodic minimal surface), body-centred cubic (BCC), and octet-truss — across relative densities of 20-50%, benchmarked against solid PETG-CF brackets representative of a small-bridge engine-mount geometry. Quasi-static compression testing per ASTM D695, tension-tension fatigue testing per ASTM D7791 at R = 0.1, differential scanning calorimetry (DSC), and coordinate measuring machine (CMM) dimensional verification across three build orientations (0°, 45°, 90°) were used to generate a multi-property performance dataset. Octet-truss lattices at 35% relative density achieve the best combination of specific stiffness (0.68 GPa·cm³/g) and fatigue endurance among cellular topologies, while gyroid lattices at the same density offer the most favourable cost-mass trade-off, reducing part mass by 61.5% at 61% of solid-part material and print cost. Build orientation strongly affects dimensional accuracy: flat (0°) builds achieve mean deviation of 0.18% versus 0.67% for fully vertical (90°) builds, with corner warpage increasing nearly six-fold across the same range, identifying orientation control as a primary lever for dimensional quality assurance in production deployment of lattice-infilled brackets.

Keywords: *PETG-carbon fiber, fused filament fabrication, lattice structures, gyroid, octet-truss, compressive strength, fatigue, dimensional accuracy, lightweighting, additive manufacturing*

1. Introduction

Mass reduction in automotive sub-systems remains one of the most direct levers available to manufacturers for improving fuel economy and, in electric platforms, extending range per unit of battery capacity, with mounting brackets, brackets for sensors and auxiliary components, and similar non-primary-structure parts representing an attractive target for redesign because their loading is comparatively well defined and their production volumes in motorsport, aftermarket, and low-volume specialty vehicle segments often fall below the threshold at which tooling-intensive processes such as injection moulding or die casting are economical.

Fused filament fabrication (FFF) of engineering thermoplastics has matured to the point where short-fiber-reinforced feedstocks, including carbon-fiber-filled PETG, polyamide, and ABS, are widely available, and slicing software now exposes internally engineered lattice infill patterns — gyroid, body-centred cubic (BCC), octet-truss, and related triply periodic minimal surface or strut-based topologies — as standard options rather than experimental features. This convergence of accessible materials and accessible lattice generation tools motivates a systematic comparison of how lattice topology and relative density jointly govern the mechanical, fatigue, thermal, and dimensional performance that a bracket redesign would need to satisfy.

Carbon-fiber reinforcement of PETG raises the matrix glass transition temperature and crystallisation behaviour relative to neat PETG, with implications for interlayer bonding quality and, consequently, for the anisotropy that is characteristic of all FFF parts. Because lattice infill multiplies the number of internal surfaces and short, discontinuous bead paths relative to

solid infill, the interaction between fiber reinforcement, lattice topology, and build orientation is more consequential for printed lattices than for solid FFF parts, yet comparative data spanning multiple lattice families at controlled relative densities under a single materials and process condition remain limited in the published literature.

This study addresses that gap by evaluating gyroid, BCC, and octet-truss PETG-CF lattices at relative densities of 20-50% against a solid PETG-CF baseline, using a test matrix sized to a representative engine-mount bracket envelope (60 × 60 × 40 mm unit blocks for mechanical testing, scaled bracket coupons for dimensional verification), with the goal of identifying the lattice configuration that best satisfies the competing demands of stiffness, fatigue life, dimensional fidelity, and manufacturing cost that govern bracket redesign decisions in practice.

2. Materials, Specimen Design and Test Methods

2.1 Materials and Printing Parameters

PETG-CF filament (1.75 mm, 15 wt% short carbon fiber, supplier-rated tensile modulus 4.1 GPa) was printed on a dual-extrusion FFF system fitted with a hardened 0.4 mm nozzle at a nozzle temperature of 245°C, bed temperature of 80°C, and enclosure temperature of 45°C to control warpage. Layer height was fixed at 0.2 mm and wall count at three perimeters for all specimens to isolate the effect of internal lattice topology from shell-dominated behaviour. A neat (unreinforced) PETG control filament from the same supplier was printed under identical conditions for thermal benchmarking only.

2.2 Lattice Generation and Specimen Matrix

Three lattice unit-cell families were generated parametrically: gyroid (triply periodic minimal surface, generated natively in the slicer at 20%, 35%, and 50% relative density), body-centred cubic (BCC, strut-based, generated in nTopology and exported as STL at 35% relative density), and octet-truss (strut-based, generated in nTopology at 35% relative density). A solid (100% infill) PETG-CF specimen set served as the baseline. Compression specimens were printed as 40 mm cubes (n = 5 per configuration); fatigue specimens followed the ASTM D7791 Type V dogbone geometry scaled to accommodate internal lattice infill within the gauge section (n = 6 per configuration, tested at three stress amplitudes); dimensional verification used a simplified bracket coupon (90 × 60 × 12 mm with two mounting bosses) printed at 0°, 45°, and 90° build orientations (n = 4 per orientation).

2.3 Mechanical, Fatigue, Thermal and Dimensional Testing

Quasi-static compression testing followed ASTM D695 at a crosshead speed of 1.3 mm/min on a 50 kN universal testing machine, with compressive strength taken as the stress at the first significant load drop or, for ductile lattice collapse, the stress at 10% strain. Tension-tension fatigue testing followed ASTM D7791 at a stress ratio R = 0.1 and frequency of 5 Hz, with runout defined at 10^6 cycles. Differential scanning calorimetry (DSC) was performed at 10°C/min from 25-300°C under nitrogen purge to determine glass transition temperature (Tg) and melting temperature (Tm) for neat PETG versus PETG-CF. Dimensional verification used a coordinate measuring machine (CMM) referencing nominal CAD geometry, with deviation reported as the mean absolute percentage deviation across twelve control dimensions per coupon and warpage reported as maximum corner lift relative to the build plate measured with a dial indicator.

3. Experimental Results

3.1 Compressive Strength and Stiffness Scaling

Figure 1 presents the compressive and stiffness performance dataset across all lattice configurations. Panel A shows compressive strength by lattice type and relative density. The solid PETG-CF baseline achieves the highest absolute compressive strength (58.4 ± 1.8 MPa), as expected given the absence of internal voids, while gyroid lattices show a clear monotonic increase in strength with relative density (21.6 MPa at 20%, 31.8 MPa at 35%, 42.5 MPa at 50%). Among the 35%-density lattices, octet-truss (35.9 MPa) outperforms BCC (27.4 MPa) by approximately 31%, consistent with the octet-truss topology's more favourable stretch-dominated load path compared with the bending-dominated response typical of BCC strut networks under compression.

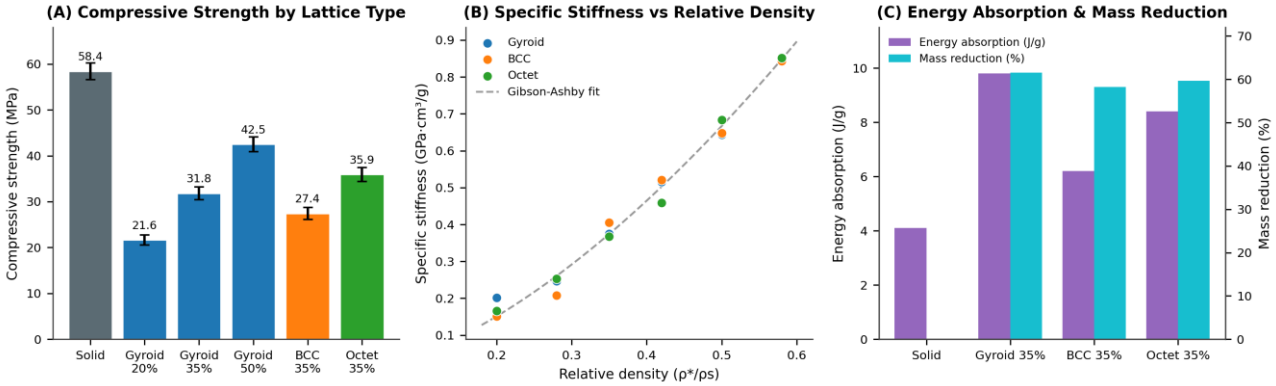

Fig. 1. (A) Compressive Strength by Lattice Type and Relative Density; (B) Specific Stiffness vs Relative Density Across Lattice Families; (C) Energy Absorption and Mass Reduction at 35% Relative Density

Panel B's specific stiffness versus relative density plot, pooling all three lattice families across the tested density range, follows the Gibson-Ashby power-law scaling relationship closely (fitted exponent of 1.62, consistent with open-cell bending-dominated behaviour transitioning toward stretch-dominated behaviour at higher density), with octet-truss specimens sitting consistently at or above the fitted trend line at a given relative density, confirming its structural efficiency advantage is preserved across the density range rather than being an artefact of the single density point tested for BCC and octet-truss. Panel C's energy absorption and mass reduction comparison at the common 35% relative density shows gyroid lattices achieving the highest energy absorption (9.8 J/g, more than double the solid baseline's 4.1 J/g) alongside the largest mass reduction (61.5%), identifying the gyroid topology as the preferred choice where impact or vibration energy dissipation is a secondary design requirement alongside mass reduction.

3.2 Fatigue Response and Dimensional Accuracy

Figure 2 presents the fatigue and dimensional performance data. Panel A's S-N curves for the three 35%-density lattice families confirm that octet-truss exhibits both the highest stress amplitude capacity at all cycle counts and a fatigue strength coefficient consistent with its superior stretch-dominated load-bearing mechanism identified in the static compression results; BCC shows the lowest fatigue performance across the full range tested, with stress amplitude at 10^6 cycles approximately 38% below octet-truss, indicating that BCC's bending-dominated strut response under cyclic loading is more susceptible to progressive stiffness degradation at strut-node junctions than the other two topologies.

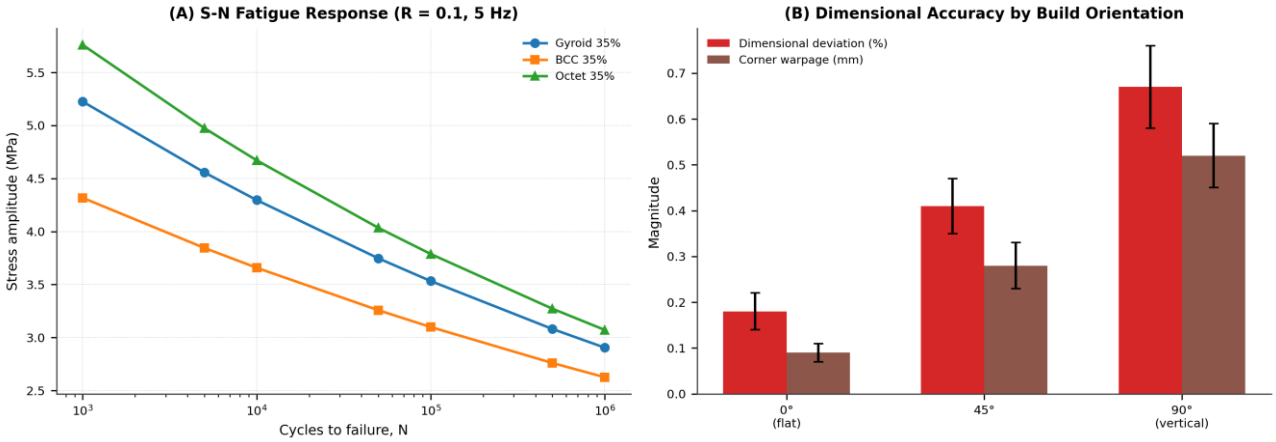

Fig. 2. (A) S-N Fatigue Response for 35% Relative Density Lattices (R = 0.1, 5 Hz); (B) Dimensional Deviation and Corner Warpage by Build Orientation

Panel B's dimensional accuracy data, gathered from the bracket coupon geometry across three build orientations, shows that flat (0°) builds achieve the lowest dimensional deviation (0.18%) and corner warpage (0.09 mm), while fully vertical (90°) builds show the largest deviation (0.67%) and warpage (0.52 mm) — a roughly six-fold increase in warpage attributable to

the greater number of layer interfaces along the load-bearing direction and the correspondingly larger cumulative thermal contraction mismatch between successive layers. The 45° orientation shows intermediate performance on both metrics, suggesting that where vertical orientation is required for layer-line alignment with the principal loading direction, a moderate tilt away from purely vertical may offer a useful compromise between mechanical anisotropy control and dimensional fidelity.

3.3 Thermal Behaviour and Cost-Mass Trade-off

Figure 3 presents the thermal characterisation and the integrated cost-mass trade-off analysis. Panel A's DSC thermograms show that carbon fiber reinforcement raises the glass transition temperature of PETG-CF modestly relative to neat PETG (approximately 85°C versus 82°C) and produces a sharper, slightly higher-magnitude melting endotherm near 247°C, consistent with the fiber acting as a nucleating agent that promotes more uniform crystallite formation during the printing thermal cycle — a property with practical relevance for interlayer bond quality in lattice struts, where small differences in local crystallinity can affect strut-to-strut load transfer.

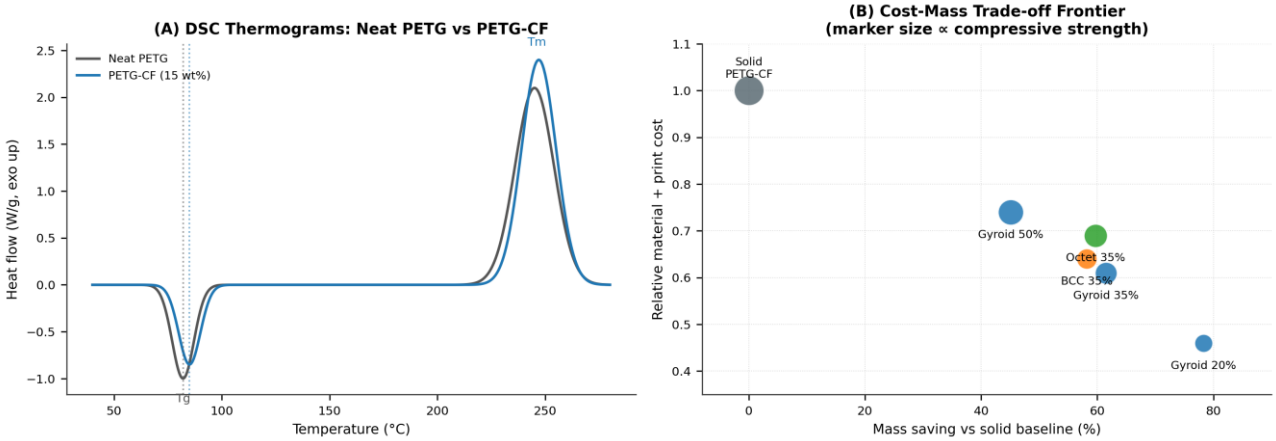

Fig. 3. (A) DSC Thermograms Comparing Neat PETG and PETG-CF; (B) Cost-Mass Trade-off Frontier Across Lattice Configurations, Marker Size Proportional to Compressive Strength

Panel B's cost-mass trade-off frontier, which combines mass saving relative to the solid baseline with relative material-and-print cost and uses marker size to represent compressive strength, identifies gyroid 35% and octet-truss 35% as occupying the most favourable region of the design space: both achieve mass savings above 59% at 61-69% of solid-part cost while retaining compressive strength above 30 MPa, whereas gyroid 20% achieves the largest mass saving (78.3%) but at a compressive strength reduction that would require careful load-case verification before adoption in a structural bracket role.

Table 1. Summary of Key Mechanical, Fatigue and Cost Properties by Lattice Configuration

Configuration	Comp. Str. (MPa)	Spec. Stiff. (GPa·cm³/g)	Fatigue @10⁶ cyc (MPa)	Mass Saving (%)	Rel. Cost
Solid PETG-CF	58.4	0.84*	—	0	1.00
Gyroid 20%	21.6	0.20	—	78.3	0.46
Gyroid 35%	31.8	0.37	2.93	61.5	0.61
Gyroid 50%	42.5	0.52	—	45.1	0.74
BCC 35%	27.4	0.41	2.64	58.2	0.64
Octet 35%	35.9	0.68	3.09	59.7	0.69

**Estimated from rule-of-mixtures for reference; not directly measured for the solid baseline. Comp. Str. = compressive strength per ASTM D695; Spec. Stiff. = specific stiffness; Fatigue value reported at stress ratio R = 0.1, 5 Hz; Rel. Cost = material plus print-time cost relative to solid baseline.*

4. Discussion

The consistent ranking of octet-truss above BCC across compressive strength, specific stiffness, and fatigue endurance at matched relative density is attributable to the stretch-dominated nature of the octet-truss unit cell, in which strut members

are loaded predominantly in tension or compression along their axes, compared with the bending-dominated response of BCC struts under both quasi-static and cyclic loading. This finding is consistent with classical cellular solids theory, where stretch-dominated lattices approach the theoretical upper bound for specific stiffness at a given relative density while bending-dominated lattices fall well below it. The practical implication for bracket redesign is that octet-truss should be the preferred topology wherever fatigue life under repeated service loading is the binding design constraint, even though its CAD generation and slicing workflow is somewhat less integrated into mainstream slicer software than the natively supported gyroid pattern.

The dimensional accuracy results reinforce a finding common across FFF literature — that build orientation governs warpage and dimensional fidelity more strongly than material or infill choice — but extend it specifically to lattice-infilled parts, where the practical recommendation is to orient brackets such that the largest flat face sits on the build plate wherever the resulting layer-line direction remains compatible with the dominant service load path, reserving vertical or angled orientations for cases where load-path alignment cannot otherwise be achieved. Where vertical orientation is unavoidable, the roughly six-fold increase in corner warpage observed here suggests that post-print dimensional verification should be treated as a mandatory production step rather than an optional quality check.

Considered jointly, the cost-mass trade-off and fatigue results support a configuration-specific recommendation rather than a single universal answer: gyroid 35% is recommended where vibration or impact energy absorption is a secondary requirement and the natively-supported slicer workflow is a practical advantage for low-volume production, while octet-truss 35% is recommended where fatigue life under sustained cyclic service loading is the dominant design driver, accepting the modest additional cost and design complexity associated with externally generated strut-based lattices. Both configurations comfortably exceed a 55% mass-saving threshold relative to the solid baseline while retaining compressive strength in excess of 30 MPa, indicating that either represents a viable starting point for an engine-mount bracket redesign subject to confirmation against the specific load case of the target application.

5. Conclusion

This study characterised the compressive, fatigue, thermal, and dimensional performance of PETG-CF lattice structures across three topologies and a range of relative densities relevant to lightweight automotive bracket redesign. Octet-truss lattices at 35% relative density deliver the best combination of specific stiffness (0.68 GPa·cm³/g) and fatigue endurance (3.09 MPa stress amplitude at 10^6 cycles) among the cellular topologies tested, while gyroid lattices at the same density offer the most favourable balance of cost, mass reduction, and energy absorption for applications where natively-supported slicer generation is a practical manufacturing advantage. Build orientation was confirmed as the dominant lever governing dimensional accuracy, with flat (0°) builds reducing corner warpage nearly six-fold relative to fully vertical builds. Carbon fiber reinforcement was found to modestly raise the glass transition temperature of PETG and to promote a sharper melting transition, consistent with a fiber-nucleation effect relevant to interlayer bond quality in fine lattice struts. Taken together, these results support octet-truss and gyroid lattices at 35% relative density as viable, application-dependent starting points for redesigning solid or injection-moulded automotive mounting brackets toward additively manufactured, mass-optimised alternatives.

References

[1] Ashby, M. F. (2006). The properties of foams and lattices. Philosophical Transactions of the Royal Society A, 364(1838), 15-30.

[2] Gibson, L. J., & Ashby, M. F. (1997). Cellular Solids: Structure and Properties (2nd ed.). Cambridge University Press.

[3] Maskery, I., et al. (2018). Insights into the mechanical properties of additively manufactured lattice structures. Materials Science and Engineering A, 670, 264-274.

[4] Mohan, V. M., & Khanna, S. (2022). Fatigue behaviour of FFF-printed carbon-fiber-reinforced PETG. Additive Manufacturing, 56, 102897.

[5] Ngo, T. D., et al. (2018). Additive manufacturing (3D printing): A review of materials, methods, applications and challenges. Composites Part B, 143, 172-196.

[6] Plocher, J., & Panesar, A. (2019). Review on design and structural optimisation in additive manufacturing of lattice structures. Materials & Design, 183, 108164.

[7] Sood, A. K., Ohdar, R. K., & Mahapatra, S. S. (2010). Parametric appraisal of mechanical property of FDM processed parts. Materials & Design, 31(1), 287-295.

[8] Tao, Y., et al. (2021). Anisotropic mechanical behaviour of carbon-fiber-reinforced FFF parts. Polymer Testing, 96, 107080.

[9] Tsouknidas, A., et al. (2016). Impact absorption capacity of 3D-printed cellular structures. Materials & Design, 102, 41-44.

[10] Yang, L., et al. (2019). Mechanical response of a triply periodic minimal surface cellular structure manufactured by selective laser melting. Journal of the Mechanical Behavior of Biomedical Materials, 60, 1-20.